



HAL
open science

Thermochemical Studies of Ni(II) and Zn(II) Ternary Complexes using Ion Mobility-Mass Spectrometry

Anna J. Corrales, Anna V Arredondo, Amber A Flores, Chloe L Duvak,
Charles L Mitchell, Riccardo Spezia, Laurence A Angel

► **To cite this version:**

Anna J. Corrales, Anna V Arredondo, Amber A Flores, Chloe L Duvak, Charles L Mitchell, et al.. Thermochemical Studies of Ni(II) and Zn(II) Ternary Complexes using Ion Mobility-Mass Spectrometry. Journal of visualized experiments : JoVE, 2022, 10.3791/63722 . hal-03775568

HAL Id: hal-03775568

<https://hal.science/hal-03775568>

Submitted on 12 Sep 2022

HAL is a multi-disciplinary open access archive for the deposit and dissemination of scientific research documents, whether they are published or not. The documents may come from teaching and research institutions in France or abroad, or from public or private research centers.

L'archive ouverte pluridisciplinaire **HAL**, est destinée au dépôt et à la diffusion de documents scientifiques de niveau recherche, publiés ou non, émanant des établissements d'enseignement et de recherche français ou étrangers, des laboratoires publics ou privés.

1 **TITLE:**

2 Thermochemical Studies of Ni(II) and Zn(II) Ternary Complexes Using Ion Mobility–Mass
3 Spectrometry

4

5 **AUTHORS AND AFFILIATIONS:**

6 Anna J. Corrales¹, Anna V. Arredondo¹, Amber A. Flores¹, Chloe L. Duvak¹, Charles L. Mitchell¹,
7 Riccardo Spezia², Laurence A. Angel¹

9 ¹Department of Chemistry, Texas A&M University-Commerce, Commerce, TX, USA

10 ²Laboratoire de Chimie Théorique, Sorbonne Université, Place Jussieu, Paris, France

11

12 Corresponding Author:

13 Laurence A. Angel (Laurence.Angel@tamuc.edu)

14

15 Email addresses of co-authors:

16 Anna J. Corrales (acorrales3@leomail.tamuc.edu)

17 Anna V. Arredondo (aarredondo10@leomail.tamuc.edu)

18 Amber A. Flores (aflores26@leomail.tamuc.edu)

19 Chloe L. Duvak (chloe.duvak@gmail.com)

20 Charles L. Mitchell (clandonmitchell@gmail.com)

21 Riccardo Spezia (ricardo.spezia@courriel.upmc.fr)

22

23 **SUMMARY:**

24 This article describes an experimental protocol using electrospray-ion mobility-mass
25 spectrometry, semi-empirical quantum calculations, and energy-resolved threshold collision-
26 induced dissociation to measure the relative thermochemistry of the dissociation of related
27 ternary metal complexes.

28

29 **ABSTRACT:**

30 This article describes an experimental protocol using electrospray-ion mobility-mass
31 spectrometry (ES-IM-MS) and energy-resolved threshold collision-induced dissociation (TCID) to
32 measure the thermochemistry of the dissociation of negatively-charged [amb+M(II)+NTA]⁻
33 ternary complexes into two product channels: [amb+M(II)]⁻ + NTA or [NTA+M(II)]⁻ + amb,
34 where M = Zn or Ni and NTA is nitrilotriacetic acid. The complexes contain one of the
35 alternative metal binding (amb) heptapeptides with the primary structures acetyl-His₁-Cys₂-
36 Gly₃-Pro₄-Tyr₅-His₆-Cys₇ or acetyl-Asp₁-Cys₂-Gly₃-Pro₄-Tyr₅-His₆-Cys₇, where the amino acids'
37 Aa_{1,2,6,7} positions are the potential metal-binding sites. Geometry-optimized stationary states of
38 the ternary complexes and their products were selected from quantum chemistry calculations
39 (presently the PM6 semi-empirical Hamiltonian) by comparing their electronic energies and
40 their collision cross-sections (CCS) to those measured by ES-IM-MS. From the PM6 frequency
41 calculations, the molecular parameters of the ternary complex and its products model the
42 energy-dependent intensities of the two product channels using a competitive TCID method to
43 determine the threshold energies of the reactions that relate to the 0 K enthalpies of
44 dissociation (ΔH_0). Statistical mechanics thermal and entropy corrections using the PM6
45 rotational and vibrational frequencies provide the 298 K enthalpies of dissociation (ΔH_{298}).

46 These methods describe an EI-IM-MS routine that can determine thermochemistry and
47 equilibrium constants for a range of ternary metal ion complexes.

48

49 INTRODUCTION:

50 This study describes a new technique using a commercially available ion mobility-mass
51 spectrometer that allows the determination of the relative thermochemistry for the
52 dissociation of an alternative metal binding (amb) ternary metal complex [amb+M(II)+NTA],
53 where M = Zn or Ni and NTA = nitrilotriacetic acid (**Figure 1**). These reactions model the
54 dissociation of the amb-tagged recombinant protein attached to the NTA-immobilized metal
55 during immobilized metal affinity chromatography (IMAC)^{1,2}. As an example, this method is
56 described using the amb heptapeptide tags of amb **A** and **H** (**Figure 2**) (chosen from the
57 previous studies³⁻¹²) that exhibit Zn(II) and Ni(II)-binding properties and, thus, have potential
58 applications as purification tags. The described process can, however, be used to evaluate
59 thermochemical energies in any organometallic system. These amb peptides have metal-
60 binding sites in the Aa₁-Aa₂ and Aa₆-Aa₇ positions that compete with the carboxylate and amine
61 sites of the NTA. The three central amb amino acids provide a spacer (Gly₃), the hinge for the
62 two arms (Pro₄), and a long-distance π -metal cation interaction (Tyr₅).

63

64 The overall 1- charge state of the [amb+M(II)+NTA]⁻ complexes is determined by the
65 protonation state of their potential binding sites. Since there is Ni(II) or Zn(II) with the 2+
66 oxidation state, there must be a net of three deprotonated negatively-charged sites. The
67 molecular modeling of the [amb+M(II)+NTA]⁻ complexes predicts that these are two protons
68 from the NTA and one proton from the amb (i.e., [amb-H+M(II)+NTA-2H]⁻). The product
69 channels contain an ionic species and a neutral species (i.e., [NTA-3H+M(II)]⁻ + amb or [amb-
70 3H+M(II)]⁻ + NTA). In the manuscript, "-3H" is excluded in the names of the complexes, but the
71 reader should know that the -3H is implied. The instrument measures the relative intensities of
72 the two ionic mass-to-charge (*m/z*) species. A major attribute of ES-IM-MS analyses is that it
73 allows the examination of the reactivity of a specific *m/z* species, as utilized here and in
74 previous amb studies³⁻¹².

75

76 Collision-induced dissociation methodologies to yield thermochemical data for large complexes
77 is a subject of significant interest^{13,14}. Methodologies including the kinetic method are not
78 conducive to fitting data over a range of energies, nor do they account for multi-collision
79 environments¹⁵⁻¹⁸. Here, the threshold CID (TCID) method, developed using guided ion beam
80 tandem mass spectrometry by Armentrout, Ervin, and Rodgers is applied¹⁹ to a new ES-IM-MS
81 instrument platform utilizing traveling-wave ion guides. The TCID method allows for relative
82 thermochemical analysis of the dissociation of the ternary complexes into their two product
83 channels and includes a threshold law describing the transfer of collision energy between the
84 translational energy of the reactant (ternary complex in this research) and an inert target gas
85 (argon in this case). The method includes integration over the reactant's internal energy
86 distribution²⁰, the translational energy distributions between the reactant and target gas²¹, and
87 the total angular momentum distributions^{22,23}. A dissociation probability and statistical Rice-
88 Ramsperger-Kassel-Marcus (RRKM) correction of the kinetic shifts resulting from the limited
89 time window for observation of the products are included²⁴. For two independent product

90 channels, the competitive TCID method allows for the simultaneous fitting of the two
91 competing product channels. Dissociation of the complex is through an orbiting transition state,
92 which has the properties of the products but is held together by a locked-dipole²⁵. The TCID
93 method is incorporated into the CRUNCH program²⁶, and the operation of the user interface is
94 described here to evaluate the thermochemistry of the two dissociation channels of the ternary
95 [amb+M(II)+NTA]⁻ complexes. The CRUNCH program is available upon request from the
96 developers²⁶.

97

98 **PROTOCOL:**

99

100 NOTE: **Figure 1** shows an overview of the protocol.

101

102 **1. Preparation of reagents**

103

104 1.1. Purchase freeze-dried amb peptides (>98% purity) and store them in a -80 °C freezer.

105

106 1.2. Purchase >99% purity zinc(II) nitrate hexahydrate and nickel(II) nitrate hexahydrate.

107

108 CAUTION: Nickel(II) nitrate hexahydrate presents an environmental and health hazard.

109

110 1.3. Purchase the nitrilotriacetic acid, poly-DL-alanine polymers, ultrapure/trace metal grade
111 ammonium acetate, ammonium hydroxide, glacial acetic acid, and HPLC grade acetonitrile.

112

113 **2. Preparation of stock solutions**

114

115 2.1. Peptide amb stock solution

116

117 2.1.1. Prepare an aqueous solution of 12.5 mM amb concentration by weighing 10–20 mg of
118 the freeze-dried peptide using no less than three significant figures and placing it in a 1.7 mL
119 polypropylene microcentrifuge tube.

120

121 2.1.2. Add the appropriate volume of deionized water (>17.8 MΩ cm) to the microcentrifuge
122 tube. Close the lid and mix well with at least 20 inversions.

123

124 2.1.3. Create 50 μL aliquots from the 12.5 mM amb solution and place them into marked 1.7 mL
125 microcentrifuge tubes. Store the aliquot stock solutions at -80 °C.

126

127 2.2. Metal ion stock solutions

128

129 2.2.1. Prepare the aqueous Zn(II) and Ni(II) solutions of 12.5 mM concentration by weighing 10–
130 30 mg of the metal nitrate hexahydrate using no less than three significant figures and placing it
131 in a 1.7 mL polypropylene microcentrifuge tube.

132

133 2.2.2. Add the appropriate amount of DI water to the microcentrifuge tube. Close the lid and

134 mix well with at least 20 inversions. Store 50 μ L aliquot stock solutions at -80°C .

135

136 2.3. NTA ion stock solutions

137

138 2.3.1. Prepare an aqueous NTA solution by weighing 10–30 mg of the NTA using no less than
139 three significant figures and placing it in a 1.7 mL microcentrifuge tube.

140

141 2.3.2. Add the appropriate amount of DI water to the NTA in the microcentrifuge tube to
142 achieve a final concentration of 12.5 mM. Close the lid and mix well with at least 20 inversions.

143

144 2.4. Ammonium acetate stock solutions: Weigh 30.8 mg of ammonium acetate and add to 40
145 mL of DI water to yield a 10 mM solution. Adjust the pH of the ammonium acetate solution to
146 pH 7.7 with 1 mM ammonium hydroxide.

147

148 2.5. Poly-DL-alanine stock solution: Make a 1 mL, 1,000 ppm poly-DL-alanine (PA) stock solution
149 by dissolving 1.0 mg of PA in DI water. Mix comprehensively. Create 50 μ L aliquots and put
150 them into individually labeled microcentrifuge tubes. Store the 1,000 ppm solution at -80°C .

151

152 **3. Electrospray-ion mobility-mass spectrometry (ES-IM-MS) collision-induced dissociation**
153 **(CID) analysis**

154

155 3.1. Prepare the instrument by cleaning the ES inlet tubing and metal capillary by injecting 500
156 μ L of 0.1 M glacial acetic acid, followed by 500 μ L of 0.1 M ammonium hydroxide, and finally
157 500 μ L of pH 7.7 ammonium acetate solution.

158

159 3.2. Liquefy the 12.5 mM amb stock solution by bringing it to room temperature. Create a final
160 concentration of 0.125 mM amb by making two successive dilutions with DI water. Mix
161 comprehensively after each dilution.

162

163 3.3. Liquefy the 12.5 mM metal ion stock solution by bringing it to room temperature. Create a
164 final concentration of 0.125 mM metal ion by making two successive dilutions with DI water.
165 Mix comprehensively after each dilution.

166

167 3.4. Liquefy the 12.5 mM NTA stock solution. Create a final concentration of 0.125 mM NTA by
168 making two successive dilutions with DI water. Mix comprehensively after each dilution.

169

170 3.5. To make a 2 mL sample of the ternary complex, add 800 μ L of 0.125 mM NTA solution and
171 400 μ L of 0.125 metal ion solution to a 2 mL microcentrifuge tube, and mix thoroughly with at
172 least 20 inversions. Add 400 μ L of ammonium acetate solution (pH 7.7) and 400 μ L of 0.125 mM
173 amb solution, mix thoroughly with at least 20 inversions, and permit the sample to equilibrate
174 for 10 min at room temperature.

175

176 **3.6. Load the 2 mL sample into a 2.5 mL blunt nose syringe and inject the sample into the ES of**
177 **the instrument using the instrument's syringe pump at a flow of 10 μ L/min.**

178

179 3.7. Place the instrument in negative IM-MS mode. Use the typical operating conditions of the
180 instrument²⁷ for these experiments as follows.

181

182 3.7.1. Inject the sample at a 10 $\mu\text{L}/\text{min}$ flow rate into the ES capillary held at -2 kV with a 500
183 L/h desolvation flow rate of nitrogen. Set the ES source and desolvation temperatures to $130\text{ }^\circ\text{C}$
184 and $263\text{ }^\circ\text{C}$, respectively. Set the sampling and extraction cones to 25 V and 3 V , respectively.

185

186 3.7.2. For the CID experiments, use the quadrupole mass analyzer to select the isotopic pattern
187 of the $[\text{amb}+\text{M}(\text{II})+\text{NTA}]^-$ ternary complex using the m/z of the monoisotopic peak with
188 resolution settings of low mass = 4.5 and high mass = 16.5.

189

190 NOTE: The $[\text{amb}+\text{M}(\text{II})+\text{NTA}]^-$ ions are passed onto the sequential three traveling wave (T-wave)
191 ion guides.

192

193 3.7.3. Ensure that the trap T-wave has an argon gas flow of $3\text{ mL}/\text{min}$ and a pressure of $2.83 \times$
194 10^{-2} mbar . Set the collision energy (CE) to the trap at 5 V to avoid any dissociation of the
195 ternary complex. Let the trap collect the ternary complex ions before releasing ($200\text{ }\mu\text{s}$ release
196 time) them into the ion mobility (IM) T-wave ion guide using a trap DC bias of 14 V , which keeps
197 dissociation of the complex at the IM entrance to a minimum.

198

199 3.7.4. Ensure that the IM ion guide has a pressure of 0.507 mbar using a $20\text{ mL}/\text{min}$ flow rate of
200 ultrapure N_2 buffer gas. Ramp the T-waves in the IM with heights of 7 V to 30 V and with
201 velocities of 290 m/s to 801 m/s for each starting and ending sweep of the IM ion guide.

202

203 3.7.5. Set the argon flow and pressure of the transfer T-wave the same as the trap T-wave. The
204 transfer T-wave was used for the collision-induced dissociation of the ternary $[\text{amb}+\text{M}(\text{II})+\text{NTA}]^-$
205 complex using the transfer CE.

206

207 3.8. Select the m/z isotope pattern of the negatively charged $[\text{amb}+\text{M}(\text{II})+\text{NTA}]^-$ complex using
208 the transmission quadrupole in resolving mode.

209

210 3.8.1. Identify the m/z isotope pattern by opening the mass spectrometry program and
211 selecting **Spectrum**. Select **Tools > Isotope model**. In the pop-up window, list the molecular
212 formula of the complex, check the box for **Show Charged Ion**, enter 1 for the charge of negative
213 one and click on **OK**.

214

215 3.8.2. In the displayed isotope pattern of the complex, note the lowest mass peak. In the
216 instrument software, select **Setup > Quad Profile**. In the window that opens, select **Manual**
217 **Fixed** and enter the mass of the lowest isotopic pattern peak. Click on **Update** and then **Close**.

218

219 3.8.3. Select **Setup** again, and then click on **Resolving Quad**. Collect the negative ion ES-IM-MS
220 spectra incrementally across a range of transfer collision energies using a 5 min run duration
221 and 2 s scan time.

222

223 NOTE: Preliminary transfer energies can be tested from 26–60 V in intervals of 2 V. The final
224 range of transfer collision energies examined should demonstrate no dissociation of the ternary
225 complex at the lowest energy and complete dissociation into the products at the highest
226 energy. For high-quality statistical analysis, this ES-IM-MS analysis should be performed for
227 each amb ternary complex at least 3x by different people and on different days to determine
228 means and standard deviations.

229

230 **4. ES-IM-MS collision cross-section (CCS) analysis**

231

232 4.1. Clean the ES inlet tubing and the metal capillary with 500 μL of 0.1 M glacial acetic acid,
233 followed by 500 μL of 0.1 M ammonium hydroxide, and finally 500 μL of pH 7.7 ammonium
234 acetate solution.

235

236 4.2. Liquefy the 1,000 ppm PA stock solution to room temperature and do two serial dilutions;
237 dilute to 100 ppm PA with DI water, and then dilute to 10 ppm PA solution by diluting with a 1:1
238 ratio of DI water and HPLC-grade acetonitrile.

239

240 4.3. Collect the negative ion IM-MS spectra of the 10 ppm PA sample for 10 min using
241 instrumental operating conditions.

242

243 NOTE: The injection flow rate and ES source conditions were the same as for the CID
244 experiments (step 3.). For measurements of the CCS, the quadrupole mass analyzer was in non-
245 resolving mode and passed all ions onto the sequential three T-wave ion guides. The operation
246 of the trap T-wave and IM T-wave ion guides was the same as for the CID experiments. The
247 collision energy of the transfer T-wave cell was at 4 V to allow ions to pass through without
248 dissociation.

249

250 4.4. Prepare each of the ternary complexes as described in steps 3.2.–3.6.

251

252 4.5. Collect the IM-MS spectra of each ternary complex for 5 min.

253

254 NOTE: Use the same instrumental conditions as in step 4.3.

255

256 4.6. Collect the negative ion IM-MS spectra of the 10 ppm PA sample for 10 min.

257

258 NOTE: The mean of the arrival times of the PA calibrants collected before and after the amb
259 ternary complexes are used in the CCS determination.

260

261 **5. Analysis of ES-IM-MS CID data**

262

263 5.1. Identify the species by matching the theoretical m/z isotope patterns of the ternary
264 complex and its products to the experimental IM-MS spectra.

265

- 266 5.1.1. Open the mass spectrometry program and select **Chromatogram** to open a new window.
267
- 268 5.1.2. In the **Chromatogram** window, click on **File > Open** to find and open the desired IM-MS
269 data file.
270
- 271 5.1.3. Right-clicking the mouse, drag across the chromatogram, and release. The MS spectrum
272 will be displayed in a separate **Spectrum** window.
273
- 274 5.1.4. In the new window displaying the spectra, select **Tools > Isotope Model**. A small window
275 will pop up. Enter the molecular formula of the amb species, check the **Show Charged Ion** box,
276 and enter the desired charge state. Click on **OK**.
277
- 278 5.1.5. To distinguish all the species in the IM-MS spectrum, repeat this process in the **Spectrum**
279 window and record their m/z isotope range.
280
- 281 5.2. For the ternary amb complex and its products, use their m/z isotope range to identify them
282 and extract their arrival time distributions (ATD).
283
- 284 5.2.1. Open the ion mobility separation software and select **File > Open** to find and open the
285 data file.
286
- 287 5.2.2. Left-click and drag with the mouse to zoom in on the m/z isotope range of the ternary
288 complex [amb+M(II)+NTA]⁻.
289
- 290 5.2.3. Using the **Selection** tool, left-click and drag to select the specific isotope range for
291 [amb+M(II)+NTA]⁻ as identified in step 5.1. Click on the **Accept Current Selection** button.
292
- 293 5.2.4. To eliminate any coincidental m/z species or background signal, use the **Selection** tool to
294 choose the ATD associated with the ternary complex. Click on the **Accept Current Selection**
295 button.
296
- 297 5.2.5. To export the ATD file to the mass spectrometry software, go to **File > Export**, and then
298 click on **Retain Drift Time**. Rename the file if desired and save the file in the appropriate folder.
299
- 300 5.3. Determine by integration of the area under the extracted ATD curve the species' relative
301 intensity.
302
- 303 5.3.1. In the **Chromatogram** window, open the saved exported file from the ion mobility
304 separation software. Select **Process** and then **Integrate**. Use a peak-to-peak amplitude setting
305 of 20 and click on **OK**.
306
- 307 5.3.2. Record the integrated area as shown on the **Chromatogram** window. Repeat steps
308 5.2.2.-5.2.5. for the two products, namely [NTA+M(II)]⁻ and [amb+M(II)]⁻.
309

310 5.3.3. Repeat steps 5.2.1.–5.3.2. for each transfer collision energy recorded.

311

312 5.4. Utilize the integrated ATD areas for the ternary complex $[\text{amb}+\text{M}(\text{II})+\text{NTA}]^-$ and two
313 products $[\text{NTA}+\text{M}(\text{II})]^-$ and $[\text{amb}+\text{M}(\text{II})]^-$ at each transfer collision energy point to normalize to a
314 relative percentage scale.

315

316 5.4.1. Create a spreadsheet by entering the identities of the ternary complex and its products
317 and their integrated ATD at each collision energy.

318

319 5.4.2. For each collision energy, utilize the summation of the integrated ATDs for $[\text{amb}+\text{M}(\text{II})$
320 $+\text{NTA}]^-$, $[\text{NTA}+\text{M}(\text{II})]^-$, and $[\text{amb}+\text{M}(\text{II})]^-$ to normalize their individual ATDs to a relative
321 percentage scale.

322

323 5.4.3. From the replicate TCID measurements, find the mean and standard deviations of each
324 data point. Convert the lab-frame transfer collision energy (E_{lab}) to the center-of-mass collision
325 energy (E_{cm}) using the average masses of the argon (m_{Ar}) collision gas and the ternary complex
326 (m_{complex}): $E_{\text{cm}} = E_{\text{lab}} (m_{\text{Ar}})/(m_{\text{Ar}} + m_{\text{complex}})$.

327

328 NOTE: E_{cm} represents the maximum energy from the collision with the argon gas, which is
329 available for dissociation of the ternary complex.

330

331 5.4.4. Plot the mean and standard deviation of the individual percentage intensities of
332 $[\text{amb}+\text{M}(\text{II})+\text{NTA}]^-$, $[\text{NTA}+\text{M}(\text{II})]^-$, and $[\text{amb}+\text{M}(\text{II})]^-$ in a graph of relative intensity (%) vs. center-
333 of-mass collision energy (eV) to exhibit how the species' relative intensities change as a
334 function of collision energy.

335

336 6. Analysis of the average arrival times for determining collision cross-sections (CCS)

337

338 6.1. Open the ion mobility separation software and the file containing the IM-MS spectrum of
339 the 10 ppm PA sample collected with the transfer collision energy set at 4 V. Extract the ATD of
340 each of the single negatively charged PA species and export the files to the mass spectrometry
341 software using the option **Retain Drift Time** (see step 5.2.5.). Repeat for the second PA
342 calibrants file.

343

344 6.2. Open the ion mobility separation software. Use **File > Open** to open one of the files
345 containing the IM-MS spectra of the amb ternary complexes recorded between the PA
346 calibrants. Extract the ATD of each of the ternary complexes and export their files to the mass
347 spectrometry software using the **Retain Drift Time** option (see step 5.2.5.).

348

349 6.3. Use a cross-sectional calibration method²⁸ to calculate the CCS of the ternary complex and
350 its products.

351

352 6.3.1. In a spreadsheet, calculate the corrected CCS (Ω_c) for each of the single negatively
353 charged PA species from their CCS (Ω)^{29,30} measured in Helium buffer gas³¹ using **Equation 1**,

354 where z = charge of the ternary complex, $e_c = 1.602 \times 10^{-19}$ C; m_{N_2} = mass of nitrogen (u), and
 355 m_{ion} = mass of ternary complex²⁸.

356

$$357 \quad \Omega_c = \frac{\Omega}{z e_c \sqrt{\left(\frac{1}{m_{N_2}} + \frac{1}{m_{ion}}\right)}} \quad (1)$$

359 6.3.2. Find the drift times (t_D) of the PA calibrants and the ternary complexes by first obtaining
 360 the average arrival times (t_A) from the maxima of the corresponding ATD curves and then
 361 applying **Equation 2**, where c = detector delay coefficient (1.41 ms; check instrument as this can
 362 vary between instruments) and m/z = mass-to-charge ratio of the PA calibrant or amb ternary
 363 complex.

364

$$365 \quad t_D = t_A - \frac{c \sqrt{m/z}}{1000} \quad (2)$$

366

367 6.3.3. Create a graph by plotting the PA calibrants' t_D vs. Ω_c . Then, using **Equation 3**, fit the data
 368 with a least-squares regression to find the constants A' and B , where A' corrects for the electric
 369 field, temperature, and pressure in the instrument and B corrects for the nonlinear behavior of
 370 the T-wave IM device.

371

$$372 \quad \Omega_c = A' t_D^B \quad (3)$$

373

374 6.3.4. Utilizing the A' and B constants and the t_D value of the amb ternary complexes, calculate
 375 their Ω_c using **Equation 3** and their Ω using **Equation 1**. The CCS values estimated by this
 376 method have absolute errors of about 2%²⁹.

377

378 7. Computational methods

379

380 7.1. Use the semi-empirical PM6³² method implemented in structural modeling and
 381 computational software³³ to locate geometry-optimized conformers of the [amb+M(II)+NTA]⁻
 382 ternary complexes and the ion and neutral product pairs: [amb+M(II)]⁻ + NTA and [NTA+M(II)]⁻
 383 + amb observed from the CID experiments. Refer to the computation visualizer usage in the
 384 **Supplementary File** for specifics on how to develop and submit calculations.

385

386 NOTE: For the present systems, the PM6 method correctly reproduced experimental data, but
 387 in general, any quantum chemistry method that is reliable and computationally doable can be
 388 used.

389

390 7.2. Run geometry optimizations and frequency calculations on multiple different starting
 391 structures to explore different conformations, protonation states, and potential binding sites.
 392 Record the electronic + zero-point energies of each of the located stationary points for each of
 393 the ternary complexes and their products.

394

395 NOTE: The starting structures for the geometry optimizations should investigate different
 396 possible combinations of binding sites and conformational arrangements. The starting
 397 structures were based on previously located B3LYP³⁴ [amb+M(II)]⁻ conformers^{3,4,6}. For
 398 [amb+M(II)+NTA]⁻, NTA was positioned to compete with the substituent sites of the amb at the
 399 Aa₁-Aa₂-Aa₆-Aa₇ and the carboxylate terminus for the singlet spin state of Zn(II) or the triplet
 400 spin state of Ni(II).

401

402 7.3. Use a program that can perform accurate collision cross-section measurements as
 403 measured in helium buffer gas (CCS_{He}) using the atomic coordinates from these quantum
 404 chemical calculations³⁵.

405

406 NOTE: Programs developed for calculating accurate CCS_{He} from peptide structures located by
 407 quantum chemical calculations include MobCal³⁶ and HPCCS^{37,38}.

408

409 7.4. Choose the lowest energy conformer exhibiting the Lennard-Jones CCS_{He} that agrees with
 410 the IM-MS-measured CCS_{He} for selecting the structures of ternary complexes and dissociation
 411 products to include in the CRUNCH modeling below.

412

413 8. CRUNCH modeling

414

415 8.1. Create a text file in the format described in the discussion section (“CRUNCH input text file
 416 format”).

417

418 NOTE: The file includes the following columns: (-1) center-of-mass collision energy (E_{cm}), (1)
 419 mean of the relative intensity of the [amb+M(II)]⁻ product, (2) standard deviation of the
 420 [amb+M(II)]⁻ intensity, (3) mean of the relative intensity of the [NTA+M(II)]⁻ product, and (4)
 421 standard deviation of the [NTA+M(II)]⁻ intensity.

422

423 8.2. Model the E_{cm} -dependent intensities of the two reaction channels [amb+M(II)+NTA]⁻ to
 424 [amb+M(II)]⁻ + NTA and [amb+M(II)+NTA]⁻ to [NTA+M(II)]⁻ + amb using the TCID technique in
 425 the CRUNCH program.

426

427 NOTE: Use the PM6 vibrational and rotational frequencies for the ternary complex and the two
 428 ion and neutral product channels. Use average masses of the ternary complex, argon collision
 429 gas, and ion and neutral products. Use values from the PM6 calculations or the NIST database
 430 for the polarizabilities (Å³) and dipole moments (Debye) for the neutral products.

431

432 8.2.1. From the CRUNCH main menu, open the text file (.GB5) containing the E_{cm} -dependent
 433 relative intensities of the products. Reply **No to read parameters.**

434

435 8.2.2. From the CRUNCH main menu, select **Modeling > Set all parameters.** From the reaction
 436 model options, choose the default **Threshold CID** option followed by **RRKM with integration
 437 over the energy transfer distribution** of the ternary complex²⁰, enter **2** for **independent
 438 product channels modeled**, and select **Calculate cross sections.** Enter **No** to **Do any two**

439 **product channels have the same ion mass?**

440

441 8.2.3. For **Product Channel # 1**, enter column [1] for the **experimental data** of the [amb+M(II)]⁻
442 product, column [2] for the **standard deviations** of the [amb+M(II)]⁻ product, column [5] for the
443 **unconvoluted model cross section**, and column [6] for the **convoluted model cross section**.
444 Enter **0** for residuals of fit.

445

446 NOTE: These column numbers correspond to the columns in the input file in step 8.1. as
447 described in the discussion (“CRUNCH input text file format”).

448

449 8.2.4. For **Product Channel # 2**, enter column [3] for the **experimental data** of the [NTA+M(II)]⁻
450 product, column [4] for the **standard deviations** of the [NTA+M(II)]⁻ product, column [7] for the
451 **unconvoluted model cross section**, and column [8] for the **convoluted model cross section**.
452 Enter **0** for residuals of fit.

453

454 8.2.5. For the **type of unconvoluted model**, choose **0 K cross section (kinetic shift included)**,
455 which includes the statistical RRKM correction of the kinetic shifts due to the 50 μs time
456 window from the collision cell to the TOF detector¹⁸.

457

458 8.2.6. For the **convolution options**, choose **Tiernan’s double integral**, which includes the
459 convolution over translational energy distributions between the ternary complex ion and the
460 argon collision gas²¹.

461

462 8.2.7. For the **numerical integration method**, choose **gaussian quadrature with pre-saved**
463 **cross sections**, followed by the number of integration points = **32**, the number of standard
464 deviations = **3.0**, and the number of standard deviations for the second integral = **3.0**.

465

466 8.2.8. The mass of ternary complex ion (u) is read automatically from the .GB5 text file,
467 followed by the mass of the collision gas (**39.948** for argon); use the defaults of **0.20 eV** for the
468 FWHM of the ion beam and **298.15 K** for gas temperature. The program automatically reads in
469 the **minimum** and **maximum** center-of-mass collision energies from the .GB5 text file; use the
470 default value for the **minimum energy increment**.

471

472 8.2.9. Use the default value for the **scaling factor Sig0**, **No** for **allow scaling of individual**
473 **product channels**, and the default values for **N** and **M**. For the **method for the g(i) calculation**,
474 choose **integrate over ro-vibrational density of states**, which includes the internal energy
475 distribution²⁰ of the ternary complex [amb+M(II)+NTA]⁻.

476

477 8.2.10. From the options for entering the molecular parameters, enter **G** to read the structural
478 modeling file³³ with the PM6 vibrational and rotational frequencies of the ternary complex.
479 Reply **Yes** to the question **is one of the reactants atomic?** Write the location and name of the
480 modeling file.

481

482 NOTE: The other options for entering the vibrational and rotational frequencies include **read**

483 **parameter file**, which will read in the parameters from a text file, or **edit/enter constants**,
484 which allows for manual entry of each parameter.

485

486 8.2.11. Scale the frequencies using the NIST-recommended PM6 scaling factor (1.062). For
487 more details on scaling, see the discussion (“scaling factors for the vibrational frequencies”).
488 The number of atoms in the ternary complex is read from the file. Reply **No** to **is the molecule**
489 **linear?** Enter the **description of the reactants** (e.g., H+Zn+NTA⁻ + Ar).

490

491 8.2.12. Enter **1** for the **charge on ion** and **1.664** for the **polarizability of the argon gas**³⁹. The
492 **mass of ion** and **mass of target** are for the ternary complex and argon, respectively, and are
493 automatically read from the .GB5 text file. Enter **0** for **harmonic vibrations**.

494

495 NOTE: The following options are for choosing different scaling factors for high or low vibrational
496 frequencies. Enter **1.062** for **high frequencies** and **0.0** for **low frequencies** (see discussion:
497 scaling factors for the vibrational frequencies). The scaled frequencies are shown. Choose **0** to
498 select **No Change**.

499

500 8.2.13. Hit Enter to read the **1-D** and **2-D rotational constants** from the structural modeling
501 file³³ entered in step 8.2.10. Select default values of **0** for the **hindered rotor treatments** and **1**
502 for **molecule symmetry**.

503

504 NOTE: The program shows the inputted data; hit Enter for **No Changes**.

505

506 8.2.14. Choose the default **300 K** for **reactant temperature**. Select **Integration** for the method
507 for **reduction of density of states array**. Select **Yes** to **truncate the energy distribution**. Enter
508 **40000 cm⁻¹** for **maximum energy for distribution**, **2.0 cm⁻¹** for **bin size**, and **32** for **number of**
509 **points in energy distribution**.

510

511 NOTE: Hit Enter 2x and check that the **truncated 32-pt array** has a population >0.9. If >0.9,
512 enter **No** to **change bins or condensation factor**. If <0.9, enter **Yes** and change the **maximum**
513 **energy for distribution** and/or **bin size**.

514

515 8.2.15. For **parameters for TCID/RRKM model**, choose **Yes** for **Change**, enter **0** for **fixed time**,
516 and **0.000050 s** for the **upper limit of the detection window**. For the utilized instrument, this is
517 the time ions take to travel from the transfer collision cell to the TOF detector and is calculated
518 using **Equation 2**.

519

520 8.2.16. For **energized molecule**, enter **C** to **copy values** from the reactants already entered.
521 Enter **-1** for source transition state (TS), **0** for destination TS, and **P** to proceed.

522

523 8.2.17. For **product channel 1**, select **1** for **single transition state** from the **dissociation channel**
524 **options** and **0** for **none** for the **sequential dissociation**. For the **transition state type**, choose **1**
525 for **orbiting**.

526

527 8.2.18. Select **G** to read the modeling program files that contain the PM6 rotational and
528 vibrational parameters for the [amb+M(II)]⁻ + NTA products. Enter **No** for **is one of the PSL TS**
529 **species atomic?** Enter the location and name of the [amb+M(II)]⁻ file. Use **1.062** for **scale**
530 **frequencies**, hit Enter for the number of atoms, and enter **No** for **is the molecule linear?**

531
532 8.2.19. Enter the location and name of the modeling file that contains the vibrational and
533 rotational frequencies for the NTA product. Use **1.062** for **scale frequencies**, hit Enter for the
534 **number of atoms**, and enter **No** for **is the molecule linear?** Enter the description of the **orbiting**
535 **TS**, e.g., H+Zn-...NTA.

536
537 8.2.20. Enter **1** for **charge of [amb+M(II)]⁻ ion**, and enter the **polarizability (16.12 Å³)** and the
538 **dipole moment (4.6183 Debye)** of NTA. Select **0 K** for **rotational temperature** and **locked-**
539 **dipole** for the treatment of the orbiting transition state. Enter the average **masses (u)** of the
540 [amb+M(II)]⁻ ion and NTA.

541
542 8.2.21. Enter **0** for **harmonic vibrations**. Enter **1.062** for **high frequencies** and **0.0** for **low**
543 **frequencies**. See the discussion section for further details of scaling frequencies; the scaled
544 frequencies are shown. Choose **0** to select **No Change**. Hit Enter to read the **1-D and 2-D**
545 **rotational constants** from the modeling files. Select **0** for **hindered rotors**, **1** for **molecule**
546 **symmetry**, and **1** for **reaction degeneracy**. Enter the **No Changes** option.

547
548 8.2.22. For **product channel 2**, select **1** for **single transition state**, **0** for **none** for the **sequential**
549 **dissociation**, and **1** for **orbiting** for the **transition state type**.

550
551 8.2.23. Select **G** to read in modeling files that contain the PM6 rotational and vibrational
552 parameters for the [NTA+M(II)]⁻ and amb products. Enter **No** for **is one of the PSL TS species**
553 **atomic?** Write the location and name of the [NTA+M(II)]⁻ modeling file.

555 8.2.24. Use **1.062** for **scale frequencies**, hit Enter to read the number of atoms, and enter **N** for
556 **is the molecule linear?** Write the location and name of the amb modeling file. Use **1.062** for
557 **scale frequencies**, hit Enter for the number of atoms, and enter **N** for **is the molecule linear?**

558
559 8.2.25. Enter the description of the **orbiting TS** (e.g., NTA+Zn-...H). Enter **1.0** for **charge of**
560 **[NTA+M(II)]⁻ ion**, and enter the **polarizability (Å³)** and the **dipole moment (Debye)** of the amb.
561 Select **0.0 K** for **rotational temperature** and **locked-dipole** for the treatment of the orbiting
562 transition state. Enter the average **masses (u)** of the [NTA+M(II)]⁻ and amb products.

563
564 NOTE: The output file contains the polarizability and dipole moments of the amb. The
565 polarizability is in units of Bohr³ and needs to be converted to the units of Å³.

566
567 8.2.26. Enter **0** for **harmonic vibrations**. Enter **1.062** for **high frequencies** and **0** for **low**
568 **frequencies**. See the discussion for more details on scaling frequencies. The scaled frequencies
569 are shown. Choose **0** to select **No Change**. Hit Enter to read the **1-D and 2-D rotational**
570 **constants** from the modeling files. Select **0** for **hindered rotors**, **1** for **molecule symmetry**, and

571 **1 for reaction degeneracy. Enter No Changes.**

572

573 **8.2.27. To handle inactive 2-D rotations, select the default options statistical angular**
574 **momentum distribution and integrate P(E,J) over J distribution.** Use the default value of **32** in
575 **the number of points in integration.**

576

577 NOTE: These selections choose the method for integration over the total angular momentum J
578 levels^{16,17}. The resulting output allows the investigator to check that all the input is correct.

579

580 8.2.28. Select the **activation energies relative to the energized molecule** option and enter
581 **relative energy** (eV) for **product channel 1** that is close to the threshold energy observed in the
582 graph of the relative intensity vs. center-of-mass collision energy of the [amb+M(II)]⁻ product
583 **(Figure 4).**

584

585 8.2.29. For **product channel 2**, enter **relative energy** (eV) that is close to the threshold energy
586 observed in the graph of the intensity vs. center-of-mass collision energy of the [NTA+M(II)]⁻
587 product. To calculate the **number of states** for each product channel, use a bin size of **2.0**. Press
588 Enter and then **No** to continue.

589

590 8.2.30. **From the Model menu, select Optimize parameters to fit data, and enter the minimum**
591 **energy and maximum energy to begin and end the data fit, respectively.**

592

593 NOTE: Use a small energy range that includes the thresholds of both channels. For further
594 details, see discussion: energy range for fitting the selected TCID model to the experimental
595 data.

596

597 8.2.31. **Select -1 for weighting modes experimental standard deviations.** Based on the data,
598 **select a minimum acceptable std. deviation** of typically 0.01 to 0.001. Select **No** for **optimized**
599 **scaling of individual channels** and **0** for the **number of iterations**.

600

601 NOTE: An alternative to using standard deviations is the **statistical** option.

602

603 8.2.32. **Use the default value for the E₀ convergence limit and select No to hold any parameter**
604 **at present value.** Enter **0.5** and **2.0** eV for the **lower and upper limits to avoid optimization**
605 **failure** and select **central finite difference** for the **derivative evaluation method**. Use the
606 default value for **numerical precision** and select **No** for **change derivative step sizes**.

607

608 NOTE: An alternative method is to select **Yes to hold any parameter at present value**. This
609 method is described further in the discussion: optimization of parameters.

610

611 8.2.33. **From the Optimization menu, select begin optimization.** The CRUNCH program will
612 **optimize the selected TCID model to the experimental data.**

613

614 NOTE: If the optimization does not find satisfactory fits, from the **changes** menu, try changing

615 the **energy range** to cover just the first few intensities rising from the thresholds. When a
 616 reasonable fit is located, increase the energy range and fit again. Other options that can help
 617 find fits to the data include choosing to **hold any parameter at present value** in **parameters**
 618 **optimized** and changing weighting options in **weights**. See the discussion for these options.

619

620 8.2.34. When a model fit to the data is found, hit Enter until the **Model** menu appears. If only
 621 part of the energy range of experimental data is fitted with the TCID model, select **Calculate**
 622 **and convolute model** to extend the model fit to all experimental collision energies.

623

624 **8.2.35. In the Model menu, select Delta H and S at T.**

625

626 NOTE: The unconvoluted CRUNCH model relates the 0 K threshold energies to the 0 K
 627 enthalpies (ΔH_0) of dissociation of the ternary complex into the two independent product
 628 channels (**Table 2**). The 298 K enthalpies (ΔH_{298}) and Gibbs free energies (ΔG_{298}) of dissociation
 629 are also derived with statistical mechanics thermal and entropy corrections using the reactant
 630 and products PM6 rotational and vibrational frequencies.

631

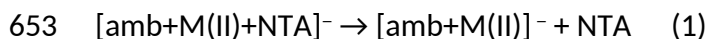
632 REPRESENTATIVE RESULTS:

633 The competitive collision-induced dissociation of the $[\text{amb}+\text{M}(\text{II})+\text{NTA}]^-$ ternary complexes of **A**
 634 and **H** into $[\text{amb}+\text{M}(\text{II})]^- + \text{NTA}$ or $[\text{NTA}+\text{M}(\text{II})]^- + \text{amb}$, are shown in **Figure 3**. The amb is shown
 635 as either **A** or **H** and the M = Zn or Ni. The $[\text{A}+\text{Zn}(\text{II})+\text{NTA}]^-$ ternary complex (**Figure 3A**) exhibits
 636 apparent thresholds of about 0.7 eV collision energy (CE) to produce $[\text{A}+\text{Zn}(\text{II})]^-$ and about 0.9
 637 eV to produce $[\text{NTA}+\text{Zn}(\text{II})]^-$. The dissociation of the $[\text{A}+\text{Ni}(\text{II})+\text{NTA}]^-$ complex (**Figure 3B**)
 638 exhibits similar thresholds (~ 1.1 eV) for both the $[\text{NTA}+\text{Ni}(\text{II})]^-$ and $[\text{A}+\text{Ni}(\text{II})]^-$ products, with
 639 $[\text{NTA}+\text{Ni}(\text{II})]^-$ increasing to 90% relative intensity, while the intensities of $[\text{A}+\text{Ni}(\text{II})]^-$ do not rise
 640 above 18%. For the $[\text{H}+\text{Zn}(\text{II})+\text{NTA}]^-$ ternary complex (**Figure 3C**), the main product is $[\text{H}+\text{Zn}(\text{II})]^-$
 641 rising from a threshold of about 0.6 eV to about 85% relative intensity, and at energies above
 642 1.0 eV, the $[\text{NTA}+\text{Zn}(\text{II})]^-$ rises to about 30%. There is also a channel for water loss from $[\text{H}-$
 643 $\text{H}_2\text{O}+\text{Zn}(\text{II})]^-$. For $[\text{H}+\text{Ni}(\text{II})+\text{NTA}]^-$ (**Figure 3D**), the $[\text{H}+\text{Ni}(\text{II})]^-$ rises from a threshold of about 0.9
 644 eV to about 40% relative intensity, while the $[\text{NTA}+\text{Ni}(\text{II})]^-$ rises from ~ 1.0 eV to about 80%.
 645 Included on the graphs is the CE where the ternary complex is 50% dissociated. The Ni(II)
 646 ternary complexes require 0.31–0.37 eV higher CE than their Zn(II) ternary complex
 647 counterparts to be 50% dissociated. This suggests the Ni(II) complexes are more stable and
 648 require higher CE to dissociate, which is further investigated using the TCID technique.

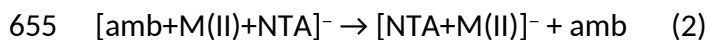
649

650 **Figure 4** illustrates the competitive TCID method, which allows for the simultaneous fitting of
 651 the two competing product channels.

652



654



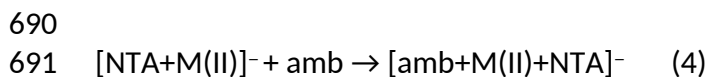
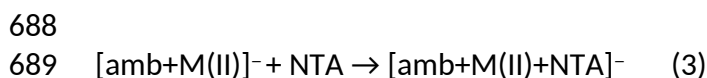
656

657 The potential energy surface (PES) illustrates the energized ternary complex dissociating into
 658 the competing product channels and shows the PM6 geometry-optimized species used to

659 model the dissociation of $[\text{amb}_H+\text{Zn(II)}+\text{NTA}]^-$. Included in the PES are the density of states of
 660 the ternary complex and the sum of states of the products. The 0 K threshold energies, E_1 and
 661 E_2 , equate to the 0 K enthalpy change for reactions 1 and 2.

662
 663 **Figure 5** shows the structures of the other three geometry-optimized ternary complexes used in
 664 this study. These species were chosen based on their predicted electronic and zero-point
 665 energies and their agreement with the IM-MS-measured collision cross-sections (CCS_{He}). **Table 1**
 666 shows there is an agreement between the ternary complexes LJ CCS_{He} and the experimental IM-
 667 MS CCS_{He} because they agree within their mutual uncertainties. The conformations of the
 668 $[\text{amb}+\text{M(II)}]$ and amb were based on the findings of our previous DFT modeling³⁻⁶. The
 669 molecular parameters of these PM6 conformers were used in the TCID modeling of the energy-
 670 resolved dissociations of the ternary complexes, including their ro-vibrational frequencies for
 671 calculating their density and sum of states.

672
 673 **Figure 6** shows the convoluted CRUNCH TCID threshold fits to the energy-resolved product
 674 intensities. The convoluted fits include the available energy and angular momentum
 675 distributions of the $[\text{amb}+\text{M(II)}+\text{NTA}]^- + \text{Ar}$ reactants. The unconvoluted fits (not shown)
 676 predicted the 0 K change in enthalpies (ΔH_0) for the dissociation of the ternary complex, and
 677 **Table 2** shows the ΔH_0 and ΔH_{298} (kJ/mol) for reactions 1 and 2. For the dissociation of the Zn(II)
 678 ternary complexes, both **A** and **H** exhibit ΔH_0 for reaction 1, which are 31 kJ/mol and [49-15](#)
 679 kJ/mol lower than the ΔH_0 for reaction 2, respectively, indicating both **A** and **H** have greater
 680 Zn(II) affinity than the NTA. The $[\text{A}+\text{Ni(II)}+\text{NTA}]^-$ ternary complex exhibits $\Delta H_0 = 146$ and 148
 681 kJ/mol for reactions 1 and 2, respectively, indicating **A** and NTA have similar affinities for Ni(II).
 682 However, the dissociation of $[\text{H}+\text{Ni(II)}+\text{NTA}]^-$ shows the ΔH_0 for reaction 1 is 36 kJ/mol lower
 683 than for reaction 2, indicating **H** has a greater Ni(II) affinity than the NTA. Overall, the
 684 $[\text{amb}+\text{Ni(II)}+\text{NTA}]^-$ complexes exhibit higher dissociation enthalpies than their $[\text{amb}+\text{Zn(II)}$
 685 $+\text{NTA}]^-$ counterparts, with the exception of **A** dissociating into $[\text{NTA}+\text{Ni(II)}]^-$. **Table 3** shows the
 686 Gibbs free energies (ΔG_{298}) of association and the formation constants (K) for the reverse
 687 reactions:



692
 693 **Table 3** demonstrates that the formation of the Ni(II) ternary complexes is more exergonic and
 694 exhibits larger formation constants K than the Zn(II) complexes ~~in all but one case~~. Reaction 4
 695 (i.e., the amb tag association with the NTA metal ion complex) is of particular interest as it
 696 represents the amb -tagged recombinant protein binding to the NTA-immobilized metal ion
 697 inside the IMAC column. Reaction 4 for the formation of $[\text{amb}_A+\text{Ni(II)}+\text{NTA}]^-$ exhibits the most
 698 spontaneous $\Delta G_{298} = -53.1$ kJ/mol and the highest formation constant, $K = 2.01 \times 10^9$.

699
 700 **FIGURE AND TABLE LEGENDS:**

701 **Figure 1: Overview of the ES-IM-MS TCID method.**

702

703 **Figure 2: The primary structures of amb A and H peptides.** Color highlights the potential
704 metal-binding sites.

705

706 **Figure 3: The center-of-mass, energy-resolved (eV) threshold collision-induced dissociation**
707 **of [amb+M(II)+NTA]⁻.** The energy-dependence of the product ions [amb+M(II)]⁻ [NTA+M(II)]⁻
708 and [amb-H₂O+Zn(II)]⁻ is shown. The center-of-mass collision energy, where there is 50%
709 dissociation of the [amb+M(II)+NTA]⁻ ternary complex, is included on the graphs.

710

711 **Figure 4: The model for the energy-resolved TCID method.** The collisions between
712 [amb_H+Zn(II)+NTA]⁻ + argon result in the dissociation to the [amb_H+Zn(II)]⁻ + NTA or
713 [NTA+Zn(II)]⁻ + amb_H products. The threshold energies E_1 and E_2 equate to the 0 K enthalpies
714 of dissociation (ΔH_0) for the reactions [amb_H+Zn(II)+NTA]⁻ → [amb_H+Zn(II)]⁻ + NTA or
715 [amb_H+Zn(II)+NTA]⁻ → [NTA+Zn(II)]⁻ + amb_H, respectively.

716

717 **Figure 5: The PM6 geometry-optimized ternary [amb+M(II)+NTA]⁻ complexes of A and H.**
718 Conformers used in the TCID modeling of the experimental data. These conformers were
719 selected from other candidate structures by comparing their PM6 electronic energies and
720 how their LJ collision cross-sections (CCS_{He}) compared to the IM-MS measured CCS_{He} .

721

722 **Figure 6: The energy-resolved, collision-induced dissociation of [amb+M(II)+NTA]⁻.** For
723 species A and H, the product ions of [amb+M(II)]⁻ and [NTA+M(II)]⁻ with the convoluted
724 CRUNCH threshold fits are shown. The energy (eV) values shown are the enthalpies of
725 dissociation at 0 K for the reactions [amb+M(II)+NTA]⁻ → [amb+M(II)]⁻ + NTA or [amb+M(II)
726 +NTA]⁻ → [NTA+M(II)]⁻ + amb.

727

728 **Figure 7: The format for the CRUNCH text input file.** The file contains the mean relative
729 intensities and their standard deviations of the product ions formed as a function of center-
730 of-mass collision energy.

731

732 **Table 1: Comparison of LJ collision cross-sections of the PM6 conformers of [amb+M(II)**
733 **+NTA]⁻.** Theoretical cross-sections of the PM6 conformers are compared with the experimental
734 CCS_{He} measured with ES-IM-MS.

735

736 **Table 2: Thermochemical results from the TCID analyses.** The energy-dependent reactions
737 [amb+M(II)+NTA]⁻ → [amb+M(II)]⁻ + NTA or [amb+M(II)+NTA]⁻ → [NTA+M(II)]⁻ + amb, showing
738 the 0 K enthalpies of dissociation (ΔH_0) derived from the unconvoluted TCID model fit, and 298
739 K enthalpies of dissociation (ΔH_{298}) derived from ΔH_0 and statistical mechanics thermal
740 corrections using the PM6 rotational and vibrational frequencies. Values are given in kJ/mol.

741

742 **Table 3: Gibbs free energies of association (ΔG_{298}) and equilibrium formation constants (K).**
743 ΔG_{298} and K at 298 K for the reverse reactions [amb+M(II)]⁻ + NTA → [amb+M(II)+NTA]⁻ and
744 [NTA+M(II)]⁻ + amb → [amb+M(II)+NTA]⁻. Derived from ΔH_{298} and statistical mechanics entropy
745 calculations using the PM6 rotational and vibrational frequencies. Values for ΔG_{298} are in kJ/mol.

746

747 DISCUSSION:**748 Critical steps**

749 **ES-IM-MS threshold collision-induced dissociation (TCID) analyses.** The TCID used the transfer
750 T-wave cell in the presence of argon as the collision cell. Prior to dissociation, the precursor ions
751 are thermalized by low-energy collisions with nitrogen gas as they pass through the ion mobility
752 (IM) cell. This results in a more reproducible energy-resolved TCID than is achieved by using the
753 trap as the collision cell^{6,40}. The thermalization of the [amb+M(II)+NTA]⁻ prior to dissociation
754 also allows the available internal energy of the ternary complex to be characterized using 298 K
755 temperature. The dissociation in the transfer cell also means the ternary complex and its
756 product ions have the same average arrival times at the detector, which was useful for
757 identifying the dissociation of the ternary complex that only occurred in the transfer cell. Other
758 regions where dissociation can occur are the ES source (sampling cone is kept at 25 V to avoid
759 this) or at the entrance of the IM cell. The product ions produced by the dissociation of the
760 ternary complex in these regions have different drift times from those produced in the transfer
761 cell because the product ions are separated from the ternary complex in the IM cell. Those
762 product ions were excluded from the analysis. In this protocol, only the integrated arrival time
763 distributions for the precursor and product ions that are co-aligned are used to determine their
764 intensities. The trap bias setting is the voltage that controls the injection voltage into the IM
765 cell, which contributes to the CID at the entrance of the IM cell. The trap bias was set at 14 V,
766 which kept the background dissociation to a minimum while not overly affecting the overall
767 intensities. A previous study⁴¹ determined the effective temperature (upper limit) of the
768 peptide dimer of leucine enkephalin to be 449 K at the entrance of the IM cell. However, the
769 effective temperature decreased rapidly as the dimer passed down the IM cell. The arrival times
770 of the amb complexes studied here exhibited Gaussian distributions, indicating they were
771 thermalized as they passed down the IM cell.

772
773 **ES-IM-MS collision cross sections (CCS) analyses.** CCS drift times were found experimentally as
774 the result of collisions with nitrogen. Those values were converted to helium-derived CCS drift
775 times using a calibration curve of known standards. This is essential as the programs used to
776 measure the CCS of the PM6 conformers require the more commonly used helium standards.

**777
778 Modifications and troubleshooting of the technique**

779 **CRUNCH input text file format.** The input text file suitable for the CRUNCH program is shown in
780 **Figure 7.** The headers in order from top to bottom are file location and version of CRUNCH;
781 date; number of energies; number of data series excluding the first energies column; source
782 file; mass of the precursor complex; mass of argon; temperature of experiment; date of
783 creation; x-data designated as -1 (the center-of-mass collision energies); and the full width at
784 half maximum (FWHM) of the ion beam. These values must be modified for each TCID
785 experiment. The FWHM energy spread of the ion beam and energy zero should be determined
786 by retarding potential analysis (RPA) by scanning the CE through low voltages and monitoring
787 the total ion current. However, under the operating conditions of the IM in the current study,
788 the ion current signal only decreased by about 50% when the transfer CE was set to its lowest
789 value. The ion beam energy zero and FWHM could be measured only upon additional
790 retardation by lowering the exit IM lens. In this latter case, the FWHM of the derivative of the

791 RPA curve gave a typical ion energy spread of 1.5 V in the lab-frame or 0.035 eV in the center-
792 of-mass frame¹³.

793

794 The pressures row relates to pressure inside the collision cell but is not used here. The
795 pressures of argon in the collision cell can be varied and the TCID data can be measured at
796 three pressures to extrapolate to single collision conditions. However, only one pressure was
797 used in this study, and the pressure results in multiple collisions. Developing the new platform
798 for a single collision is an area of ongoing research. Masses relate to the two product ions
799 whose intensities are in the columns below. Dwells can be left as default. The five columns are
800 the center-of-mass collision energies (designated -1); the mean of the ion intensities of the
801 species with mass 898.30 u; the standard deviations of the ion intensities of species 898.30 u;
802 the mean of the ion intensities of the species with mass 253.53 u; and the standard deviations
803 of the ion intensities of species 253.53 u.

804

805 **Molecular Modeling**

806 The number of conformers were narrowed initially by using models derived from previous
807 studies⁹⁻¹³. CRUNCH fitting requires careful screening of reactants, activated molecules, and
808 transition states to obtain accurate threshold energies. Previous research⁹⁻¹³ has included
809 extensive screening of [amb+M(II)] conformers to obtain the structures with the parameters
810 used in the CRUNCH modeling here. Only complexes with *trans* peptide bonds were used
811 because only they are in agreement with IM-MS measured CCS_{He}¹⁰. The B3LYP and PM6
812 molecular modeling methods both predict the lowest energy [amb+M(II)]⁻ conformer that
813 exhibits Aa₁-Cys₂-Cys₇ and carboxylate terminus coordination of Zn(II) or Ni(II)¹⁰⁻¹³. Familiarity
814 with the behaviors of the known models allowed for the new conformers of [amb+M(II)+NTA]⁻
815 to be determined more efficiently. To assist in conformer determination, as lower energy
816 conformers were located by the PM6 method, they were filtered out and reassessed
817 systematically until the most feasible, lowest energy conformers remained.

818

819 **CRUNCH modeling**

820 **Time-window for observing dissociation.** In this study, the 50 μs time window from the
821 beginning of the transfer cell to the end of the TOF analyzer, where the multichannel plate
822 detector is positioned, was used. It may be better to use the experimental time window
823 between activation in the transfer cell and the entrance to the TOF mass analyzer because, if
824 the activated ion dissociates during its time in the reflectron TOF, this metastable decay will be
825 measured at a different *m/z*. However, in this study, the product ions observed in the mass
826 spectra were all identifiable as the unmodified *m/z* species shown in **Figure 3**. This indicates
827 that metastable decay was not an issue. Further research could investigate this by examining a
828 known reaction with a high threshold and checking that the correct threshold energy is
829 obtained using the 50 μs time window and RRKM modelling.

830

831 **Scaling factors for the vibrational frequencies.** The NIST-recommended scaling factors for PM6
832 (1.062) vibrational frequencies were used. These were satisfactory for fitting the [A+Zn(II)
833 +NTA]⁻, [A+Ni(II)+NTA]⁻, and [H+Zn(II)+NTA]⁻ data. For some cases where the higher energy
834 channel is entropically favored over the lower energy channel, it may be necessary to

835 additionally scale the frequencies of the second channel. One approach is to scale the
836 frequencies below 900 cm^{-1} (as these are the least accurate) to loosen the frequencies and
837 make the TS more entropically favored.

838

839 **Optimization of parameters.** Using the **Yes** option to **Hold any parameter at present value** can
840 be helpful to fit the data successfully. For the first fit, the $E_0(2)$ is held and the model TCID is
841 fitted to the data by optimizing the CONST, $E_0(1)$, and N variables. Once a good fit is located, the
842 **parameters** option and **Hold any parameter at present value** can be used to hold CONST, $E_0(1)$,
843 and N, while allowing $E_0(2)$ to optimize to the data. Finally, once $E_0(2)$ is optimized, in the
844 **parameters** option, all four parameters CONST, $E_0(1)$, $E_0(2)$, and N should be allowed to
845 optimize to the data.

846

847 **Energy range for fitting the selected TCID model to the experimental data.** The energy range
848 used to fit the experimental data should reproduce as much of the experimental intensity data
849 as possible while maintaining a good fit in the threshold region. One can start by fitting the TCID
850 model to a small energy range at the thresholds of the experimental data. One can choose a
851 starting energy that exhibits the background intensity just prior to the rising intensity threshold
852 behavior. Once the TCID fit is optimized to the experimental data range, the range should be
853 increased by 0.1 eV and the fit should be optimized again. This procedure should be repeated
854 to fit as much of the data range as possible while maintaining the fit of the threshold region.

855

856 **Thermochemical Analyses.** The thermochemical results from **Delta H and S at T** option should
857 be compared with a series of different energy range fits to the data to estimate the standard
858 deviation of the TCID model fit. Fits to compare should include smaller ranges that fit the initial
859 rising threshold intensities well with those with greater ranges that include the higher energies
860 as well.

861

862 **ACKNOWLEDGMENTS:**

863 This material is based upon work supported by the National Science Foundation under
864 1764436, NSF REU program (CHE-1659852), NSF instrument support (MRI-0821247), Physics
865 and Astronomy Scholarship for Success (PASS) NSF project (1643567), Welch Foundation (T-
866 0014), and computing resources from the Department of Energy (TX-W-20090427-0004-50) and
867 L3 Communications. The authors thank Kent M. Ervin (University of Nevada - Reno) and Peter B.
868 Armentrout (University of Utah) for sharing the CRUNCH program and for advice on fitting from
869 PBA. The authors thank Michael T. Bower's group at the University of California - Santa Barbara
870 for sharing the Sigma program.

871

872 **DISCLOSURES:**

873 The authors have no conflict of interest to disclose.

874

875 **REFERENCES:**

876 1. Kim, Y. -M., Chen, P. Ligand binding energy in $[(\text{bipy})\text{Rh}(\text{P}\equiv\text{CH})]^+$ by collision-induced
877 dissociation threshold measurements. *International Journal of Mass Spectrometry*. **202** (1-3),
878 1-7 (2000).

- 879 2. Plattner, D. Electrospray mass spectrometry beyond analytical chemistry: Studies of
880 organometallic catalysis in the gas phase. *International Journal of Mass Spectrometry*. **207** (3),
881 125–144 (2001).
- 882 3. Narancic, S., Bach, A., Chen, P. Simple fitting of energy-resolved reactive cross sections
883 in threshold collision-induced dissociation (T-CID) experiments. *Journal of Physical Chemistry A*.
884 **111** (30), 7006–7013 (2007).
- 885 4. Ervin, K., Armentrout., P. B., Systematic and random errors in ion affinities and
886 activation entropies from the extended kinetic method. *Journal of Mass Spectrometry*. **39** (9),
887 1004–1015 (2004).
- 888 5. Cooks, R. G., Wong, P. S. H., Kinetic method of making thermochemical determinations:
889 Advances and applications. *Accounts of Chemical Research*. **31** (7), 379–386 (1998).
- 890 6. Ervin, K., Microcanonical analysis of the kinetic method. The meaning of the “apparent
891 entropy”. *Journal of the American Society of Mass Spectrometry*. **13** (5), 435–452 (2002).
- 892 7. Amarasinghe, C., Jin, J.-P. The use of affinity tags to overcome obstacles in recombinant
893 protein expression and purification. *Protein & Peptide Letters*. **22** (10), 885–892 (2015).
- 894 8. Bornhorst, J. A., Falke, J. J. Purification of proteins using polyhistidine affinity tags.
895 *Methods in Enzymology*. **326**, 245–254 (2000).
- 896 9. Yousef, E. N., Angel, L. A. Comparison of the pH-dependent formation of His and Cys
897 heptapeptide complexes of nickel(II), copper(II), and zinc(II) as determined by ion mobility-mass
898 spectrometry. *Journal of Mass Spectrometry*. **55** (3), e4489 (2020).
- 899 10. Lin, Y.-F. et al. Weak acid-base interactions of histidine and cysteine affect the charge
900 states, tertiary structure, and Zn(II)-binding of heptapeptides. *Journal of the American Society of*
901 *Mass Spectrometry*. **30**, 2068–2081 (2019).
- 902 11. Wagoner, S. M. et al. The multiple conformational charge states of zinc(II) coordination
903 by 2His-2Cys oligopeptide investigated by ion mobility - mass spectrometry, density functional
904 theory and theoretical collision cross sections. *Journal of Mass Spectrometry*. **51** (12), 1120–
905 1129 (2016).
- 906 12. Flores, A. A. et al. Formation of Co(II), Ni(II), Zn(II) complexes of alternative metal
907 binding heptapeptides and nitrilotriacetic acid: Discovering new potential affinity tags.
908 *International Journal of Mass Spectrometry*. **463**, 116554 (2021).
- 909 13. Flores, A. A. et al. Thermochemical and conformational studies of Ni(II) and Zn(II)
910 ternary complexes of alternative metal binding peptides with nitrilotriacetic acid. *International*
911 *Journal of Mass Spectrometry*. **473**, 116792 (2022).
- 912 14. Sesham, R. et al. The pH dependent Cu(II) and Zn(II) binding behavior of an analog
913 methanobactin peptide. *European Journal of Mass Spectrometry*. **19** (6), 463–473 (2013).
- 914 15. Choi, D. et al. Redox activity and multiple copper(I) coordination of 2His-2Cys
915 oligopeptide. *Journal of Mass Spectrometry*. **50** (2), 316–325 (2015).
- 916 16. Vytla, Y., Angel, L. A. Applying ion mobility-mass spectrometry techniques for explicitly
917 identifying the products of Cu(II) reactions of 2His-2Cys motif peptides. *Analytical Chemistry*. **88**
918 (22), 10925–10932 (2016).
- 919 17. Yousef, E. N. et al. Ion mobility-mass spectrometry techniques for determining the
920 structure and mechanisms of metal ion recognition and redox activity of metal binding
921 oligopeptides. *Journal of Visualized Experiments*. (151), e60102 (2019).
- 922 18. Ilesanmi, A. B., Moore, T. C., Angel, L. A. pH dependent chelation study of Zn(II) and

- 923 Ni(II) by a series of hexapeptides using electrospray ionization - Ion mobility - Mass
924 spectrometry. *International Journal of Mass Spectrometry*. **455**, 116369 (2020).
- 925 19. Armentrout, P. B., Ervin, K. M., Rodgers, M. T. Statistical rate theory and kinetic energy-
926 resolved ion chemistry: Theory and applications. *Journal of Physical Chemistry A*. **112** (41),
927 10071-10085 (2008).
- 928 20. Dalleska, N. F., Honma, K., Sunderlin, L. S., Armentrout, P. B. Solvation of transition
929 metal ions by water. Sequential binding energies of $M+(H_2O)_x$ ($x = 1-4$) for $M = Ti$ to Cu
930 determined by collision-induced dissociation. *Journal of the American Chemical Society*. **116** (8),
931 3519-3528 (1994).
- 932 21. Ervin, K. M., Armentrout, P. B. Translational energy dependence of $Ar^+ + XY \rightarrow ArX^+ + Y$
933 ($XY = H_2, D_2, HD$) from thermal to 30 eV c.m. *Journal of Chemical Physics*. **83**, 166-189 (1985).
- 934 22. DeTuri, V. F., Ervin, K. M. Competitive threshold collision-induced dissociation: Gas-
935 phase acidities and bond dissociation energies for a series of alcohols. *Journal of Physical*
936 *Chemistry A*. **103** (35), 6911-6920 (1999).
- 937 23. Iceman, C., Armentrout, P. B. Collision-induced dissociation and theoretical studies of K^+
938 complexes with ammonia: a test of theory for potassium ions. *International Journal of Mass*
939 *Spectrometry*. **222** (1-3), 329-349 (2003).
- 940 24. Rodgers, M. T., Ervin, K. M., Armentrout, P. B. Statistical modeling of collision-induced
941 dissociation thresholds. *Journal of Chemical Physics*. **106**, 4499-4508 (1997).
- 942 25. Rodgers, M. T., Armentrout, P. B. Statistical modeling of competitive threshold collision-
943 induced dissociation. *Journal of Chemical Physics*. **109**, 1787-1800 (1998).
- 944 26. Armentrout, P. B., Ervin, K. M. CRUNCH, Fortran program, version 5.2002 (2016).
- 945 27. Pringle, S. D. et al. An investigation of the mobility separation of some peptide and
946 protein ions using a new hybrid quadrupole/travelling wave IMS/oa-ToF instrument.
947 *International Journal of Mass Spectrometry*. **261** (1), 1-12 (2007).
- 948 28. Smith, D. P. et al. Deciphering drift time measurements from travelling wave ion
949 mobility spectrometry-mass spectrometry studies. *European Journal of Mass Spectrometry*. **15**
950 (2), 113-130 (2009).
- 951 29. Forsythe, J. G. et al. Collision cross section calibrants for negative ion mode traveling
952 wave ion mobility-mass spectrometry. *Analyst*. **140** (20), 6853-6861 (2015).
- 953 30. Allen, S. J., Giles, K., Gilbert, T., Bush, M. F. Ion mobility mass spectrometry of peptide,
954 protein, and protein complex ions using a radio-frequency confining drift cell. *Analyst*. **141** (3),
955 884-891 (2016).
- 956 31. Salbo, R. et al. Traveling-wave ion mobility mass spectrometry of protein complexes:
957 accurate calibrated collision cross-sections of human insulin oligomers. *Rapid Communications*
958 *in Mass Spectrometry*. **26** (10), 1181-1193 (2012).
- 959 32. Stewart, J. J. P. Optimization of parameters for semiempirical methods V: Modification
960 of NDDO approximations and application to 70 elements. *Journal of Molecular Modeling*. **13**,
961 1173-1213 (2007).
- 962 33. Frisch, M. J. et al. Gaussian 09, Revision C.01. Wallingford CT: Gaussian, Inc (2012).
- 963 34. Becke, A. D. Density-functional thermochemistry. III. The role of exact exchange. *Journal*
964 *of Chemical Physics*. **98**, 5648-5652 (1993).
- 965 35. Wyttenbach, T., von Helden, G., Batka, J. J., Jr., Carlat, D., Bowers, M. T. Effect of the
966 long-range potential on ion mobility measurements. *Journal of the American Society of Mass*

- 967 *Spectrometry*. **8**, 275–282 (1997).
- 968 36. Shvartsburg, A. A., Jarrold, M. F. An exact hard-spheres scattering model for the
969 mobilities of polyatomic ions. *Chemical Physics Letters*. **261** (1-2), 86–91 (1996).
- 970 37. Heerdt, G., Zanutto, L., Souza, P. C. T., Araujo, G., Skaf, M. S. Collision cross section
971 calculations using HPCCS. *Methods in Molecular Biology*. **2084**, 297–310 (2020).
- 972 38. Zanutto, L., Heerdt, G., Souza, P. C. T., Araujo, G., Skaf, M. S. High performance collision
973 cross section calculation-HPCCS. *Journal of Computational Chemistry*. **39** (21), 1675–1681
974 (2018).
- 975 39. <https://cccbdb.nist.gov/pollistx.asp>
- 976 40. Raja, U. K. B., Injeti, S., Culver, T., McCabe, J. W., Angel, L. A. Probing the stability of
977 insulin oligomers using electrospray ionization ion mobility mass spectrometry. *European*
978 *Journal of Mass Spectrometry*. **21** (6), 759–774 (2015).
- 979 41. Merenbloom, S. I., Flick, T. G., Williams, E. R. How hot are your ions in TWAVE ion
980 mobility spectrometry? *Journal of the American Society of Mass Spectrometry*. **23** (3), 553–562
981 (2012).
- 982